

Collision Spectroscopy. IV. Semiclassical Theory of Inelastic Scattering with Applications to $\text{He}^+ + \text{Ne}$

R. E. Olson and F. T. Smith*

Stanford Research Institute, Menlo Park, California 94025

(Received 28 October 1970)

A two-state semiclassical theory of elastic and inelastic scattering is formulated and compared to the Stueckelberg-Landau-Zener, distorted-wave, and close-coupled two-state methods. The semiclassical theory is shown to explain the physical origin of oscillatory structure on both the elastic and inelastic differential cross sections, and of a rainbowlike structure in the elastic scattering. Using simple and plausible interactions, theoretical elastic and inelastic differential cross sections are calculated and compared to the experimental measurements of the elastic and inelastic differential cross sections for $\text{He}^+ + \text{Ne}$. The scattering is characterized by a ${}^2\Sigma - {}^2\Sigma$ crossing located at $r_x = 2.02$ a.u. with an energy $E_x = 0.530$ a.u., leading to the final state $\text{He}^+ + \text{Ne}^*$ ($2p^5 3s$). The interaction energy at the crossing is found to be $V_{12}(r_x) = 0.0082$ a.u.

INTRODUCTION

A considerable volume of experimental information is becoming available on the processes of elastic and inelastic scattering of ions and atoms, including the detailed angle and energy dependence of various cross sections. Naturally, only a small number of *ab initio* calculations are available for comparison with the experimental results. In general, experimental measurements, unlike calculations, can be carried out just as easily using heavy atoms as light ones. In order to exploit this available experimental information and turn it into useful understanding of the interatomic interactions responsible for the scattering, we are making extensive use of methods of analysis based on semiclassical ideas.

In scattering at small and moderate angles, which is usually the most convenient region for experimental observations because of favorable signal-to-background ratios, presentation and analysis of the data is particularly convenient if one expresses the energy and angular dependence of the differential cross section $\sigma(E, \theta)$ in terms of the energy E and the angle of scattering θ by using the reduced scattering angle $\tau = E\theta$, which depends only on the impact parameter b (except for small corrections if θ becomes large), and the reduced cross section $\rho = \theta \sin\theta \sigma(E, \theta)$, which similarly depends mostly on the impact parameter, i.e., on τ itself. When the scattering is simple and uncomplicated by quantal interference patterns, such a reduced plot of elastic scattering data allows the potential responsible for the scattering to be deduced purely from the experimental data.

However, in most cases, the scattering is not so simple, and the differential scattering patterns commonly show oscillating features of several types

that share certain general characteristics of regularity. In general, they represent interference patterns and can be related semiclassically to the existence of two or more trajectories resulting in scattering at the same observed angle and at the same final velocity. Such patterns are observed both in elastic and in inelastic scattering.

One of the commonest sources of these interference patterns is the crossing of two electronic states of the combined system. This leads to inelastic transitions, the probability for which is often governed by the well-known Landau-Zener-Stueckelberg theory. Characteristic of these interactions in general is the fact that the transition occurs with significant probability only near the crossing point, and that a transition between states may occur either on the inbound passage or on the outbound passage at the crossing point. The result is two possible trajectories leading to the same final state, and therefore a quantal interference pattern as the angle of scattering or the energy is changed. Such oscillating patterns have been seen both in inelastic scattering and in the companion elastic scattering (where one trajectory involves no transitions at the crossing, and the other involves two). Two significant types of information are available from these inelastic scattering patterns and elastic perturbations. These are the spacing of the oscillations and their amplitudes, both of which commonly show significant regularities as functions of energy and angle. The regularities in spacing can be well displayed if one numbers peaks by successive integers N and plots as a function of τ a quantity defined by $\alpha(\tau) = 2\pi(N + N_0)\hbar v$, where N_0 can be determined either theoretically or by adjusting the experimental data so that the results at different energies fall into a common pattern. Here, v is the collision velocity. The quantity $\alpha(\tau)$ itself is a semiclassical

quantity that represents essentially a reduced action integral and controls the principal part of the relative phase of the two components of the scattering amplitude. Like τ and ρ , $\alpha(\tau)$ is essentially a function of the impact parameter only (except for small corrections) and therefore is uniquely related to τ itself. The quantity N_0 is a quantal contribution to the relative phase and may be genuinely constant, or it may in fact vary slowly with E and b . From the behavior of the function $\alpha(\tau)$, as well as from ρ , much information can be obtained about the potentials governing the trajectories participating in the scattering, including information on the locations of the crossings responsible for the inelastic transitions. When oscillations of more than one type are superimposed, their analysis presents greater difficulty, but with patience, luck, and plenty of data many of these situations can be successfully disentangled.

The amplitudes of the oscillating patterns associated with crossings contain important information about the energy associated with the coupling between the states. The Landau-Zener formula is a simple and very useful approximation to the correct theory and often allows the magnitude of this coupling matrix element to be extracted from the velocity dependence of the transition probability. As we shall see, the detailed behavior of the amplitude as a function of angle, as well as energy, involves other factors as well as the Landau-Zener transition probability.

The above concepts have been applied in the analysis of several pieces of experimental information, including elastic and inelastic scattering of He^+ by Ne and Ar , and Li^+ by Li .¹ Other information is still being analyzed.

The use of semiclassical theory in these analyses of experimental data is soundly based on quantum mechanics, and the proofs have been developed in a variety of ways, including Feynman's approach to quantum mechanics through the use of action integrals,² the WKB approximation,³ eikonal approximations,⁴ the Lippmann-Schwinger method using integral equations,⁵ the wave packet approximation,⁶ and the ordinary procedures derived from Schrödinger's version of quantum mechanics requiring the solution of coupled differential equations. In a very important series of papers, Delos and Thorson are now publishing a definitive study on the foundations and validity of the semiclassical method as well as on the Landau-Zener approximation for inelastic processes.⁷

The semiclassical procedure in scattering problems consists in approximating the scattering amplitude by a sum over one or more complex terms, each of which arises from a well-defined classical trajectory between the initial and the final states; the squared absolute magnitude of each term is just

the classical contribution to the cross section arising from that trajectory, and the phase of each complex term is determined by the classical action integral over the trajectory in question, divided by \hbar . Semiclassical procedures thus make the greatest possible use of quantities computed classically in order to express typical quantal phenomena such as interference patterns, and the expressions involved are often extremely good approximations to the true quantal solution. Further improvements can sometimes be made by using the procedure which we have termed semiquantal, in which cross sections are computed by an explicit summation over partial waves, but the phase shifts for each value of l are computed classically. (The so-called "WKB phase shift" is identically a classical quantity, and in fact the WKB procedure merely provides a proof that the classical expression is a good approximation to the quantal phase shift.)

In this paper we shall concern ourselves with the systematic development of the semiclassical method as applied to curve crossings and the resulting inelastic scattering and elastic perturbations. We develop methodically the semiclassical expressions for scattering involving the various elastic and inelastic trajectories using the Stueckelberg-Landau-Zener theory for the crossing, and we compare the results with two-state calculations using the distorted wave approximation and a close-coupled calculation of the transition probabilities from the differential equations. The results are applied to the specific case of $\text{He}^+ + \text{Ne}$.

THEORY

A. Semiclassical

Consider a crossing at r_x between two states with potentials $V_1(r)$ and $V_2(r)$ such that $V_1 > V_2$ for $r < r_x$, $V_1 < V_2$ for $r > r_x$, and with an interaction $V_{12}(r)$ that is small compared to the separation $\Delta V = V_1 - V_2$ except in a small region $r_x \pm \delta r_x$.

Outside the crossing region, i. e., when

$$|r - r_x| \gtrsim \delta r_x = V_{12}(r_x) / |\Delta V'(r_x)|,$$

the particles can be thought of as traveling on an essentially classical trajectory controlled by one of the individual potentials V_1 or V_2 . Switching from one trajectory to another occurs only near the crossing point r_x . If the turning point (and, in general, the impact parameter) is less than $r_x - \delta r_x$, there are several trajectories available, two elastic ones (T_I following the potential V_1 everywhere, T_{II} following V_1 for $r > r_x$ and following V_2 for $r < r_x$) and two inelastic [T_{III} following V_1 all the way in to the turning point r_1 and out again to r_x where it switches to V_2 for the rest of the outward passage, and T_{IV} following V_1 only to the first (inward) passage past r_x and switching to V_2 for all the rest of

the encounter]. As long as the turning points r_1 and r_2 fall outside the crossing region $r_x \pm \delta r_x$, a semiclassical treatment of the collision parameters is feasible; when the turning points approach r_x too closely, threshold effects occur that require more detailed quantal analysis.

To discuss the scattering pattern, we need to know the deflection function $\Theta_J(L, E)$ ($J=I, II, III, IV$) for each of the trajectories, and the corresponding classical action integrals $A_J(L, E)$. The Θ_J can be expressed as linear combinations of the ordinary deflection functions

$$\Theta_i(L, E) = \pi - 2b_i \times \int_{r_i}^{\infty} \left(1 - \frac{V_i(r) - V_i(\infty)}{E - V_i(\infty)} - \frac{b_i^2}{r^2} \right)^{-1/2} \frac{dr}{r^2} \quad (1)$$

(r_i is the outermost zero of the integrand, and b_i is the impact parameter), or their average

$$\Theta_d(L, E) = \frac{1}{2}[\Theta_1(L, E) + \Theta_2(L, E)], \quad (2)$$

and of the special deflection functions reflecting the contributions inside r_x

$$\Theta_i(L, E, r_x) = -2b_i \times \int_{r_i}^{r_x} \left(1 - \frac{V_i(r) - V_i(\infty)}{E - V_i(\infty)} - \frac{b_i^2}{r^2} \right)^{-1/2} \frac{dr}{r^2}, \quad (3)$$

which always appear in the combination

$$\Theta_d(L, E) = \frac{1}{2}[\Theta_1(L, E, r_x) - \Theta_2(L, E, r_x)]. \quad (4)$$

The b_i are related to the orbital angular momentum L by

$$L^2 = 2\mu[E - V_i(\infty)]b_i^2. \quad (5)$$

The Θ_J are then

$$\begin{aligned} \Theta_I(L, E) &= \Theta_1(L, E), \\ \Theta_{II}(L, E) &= \Theta_1(L, E) - 2\Theta_d(L, E), \\ \Theta_{III}(L, E) &= \Theta_d(L, E) + \Theta_d(L, E), \\ \Theta_{IV}(L, E) &= \Theta_d(L, E) - \Theta_d(L, E). \end{aligned} \quad (6)$$

The action integrals A_J are exactly the same sorts of combinations of the ordinary action integrals

$$\begin{aligned} A_i(L, E) &= 2\{2\mu[E - V_i(\infty)]\}^{1/2} \\ &\times \lim_{R \rightarrow \infty} \left[\int_{r_i}^R \left(1 - \frac{V_i(r) - V_i(\infty)}{E - V_i(\infty)} \right) \right. \\ &\times \left. \left(1 - \frac{V_i(r) - V_i(\infty)}{E - V_i(\infty)} - \frac{b_i^2}{r^2} \right)^{-1/2} dr - R \right], \end{aligned} \quad (7)$$

and of the special action integrals

$$\begin{aligned} A_i(L, E, r_x) &= 2\{2\mu[E - V_i(\infty)]\}^{1/2} \\ &\times \int_{r_i}^{r_x} \left(1 - \frac{V_i(r) - V_i(\infty)}{E - V_i(\infty)} \right) \\ &\times \left(1 - \frac{V_i(r) - V_i(\infty)}{E - V_i(\infty)} - \frac{b_i^2}{r^2} \right)^{-1/2} dr. \end{aligned} \quad (8)$$

The functions $\Theta_i(L, E)$ and $A_i(L, E)$ can be expanded in powers of $[E - V_i(\infty)]^{-1}$ by an established procedure,⁸ a variant of which can also be used to obtain expansions of $\Theta_i(L, E, r_x)$ and $A_i(L, E, r_x)$. If we define

$$\begin{aligned} G_n^i(r) &= \frac{1}{n!} [E - V_i(\infty)]^{-n} \frac{d^n}{d(r^2)^n} \\ &\times \{r^{2n-2} [V_i(r) - V_i(\infty)]^n\}, \end{aligned} \quad (9)$$

the usual expansions are

$$\Theta_i(L, E) = -2b_i \sum_{n=1}^{\infty} \int_b^{\infty} \frac{G_n^i(r) r dr}{(r^2 - b_i^2)^{1/2}}, \quad (10)$$

$$A_i(L, E) = 2\{2\mu[E - V_i(\infty)]\}^{1/2} \sum_{n=1}^{\infty} \int_b^{\infty} \frac{G_n^i(r) r^3 dr}{(r^2 - b_i^2)^{1/2}}. \quad (11)$$

The special functions can be written in a similar form if we use the upper limit

$$z_i = r_x \left(1 - \frac{V_i(r_x) - V_i(\infty)}{E - V_i(\infty)} \right)^{1/2}. \quad (12)$$

But, unlike Eqs. (10) and (11), the leading term ($n=0$) of the expansion does not vanish:

$$\Theta_i(L, E, r_x) = -2b_i \sum_{n=0}^{\infty} \int_{b_i}^{z_i} \frac{G_n^i(r) r dr}{(r^2 - b_i^2)^{1/2}}, \quad (13)$$

$$\begin{aligned} A_i(L, E, r_x) &= 2\{2\mu[E - V_i(\infty)]\}^{1/2} \\ &\times \sum_{n=0}^{\infty} \int_{b_i}^{z_i} \frac{G_n^i(r) r^3 dr}{(r^2 - b_i^2)^{1/2}}. \end{aligned} \quad (14)$$

The successive terms of Θ_i and A_i can in turn be expanded in powers of E^{-1} ; it is convenient first to introduce a standard impact parameter defined by

$$b^2 = L^2/2\mu E. \quad (15)$$

For the $n=0$ terms we get

$$\begin{aligned} \Theta_i^{n=0}(L, E, r_x) &= -2 \cos^{-1}(b_i/z_i) \\ &= -2 \cos^{-1} \left(\frac{b}{r_x} \right) + \frac{V(r_x) b}{2E(r_x^2 - b^2)^{1/2}} \\ &\quad + \mathcal{O} \left(\frac{1}{E^2} \right), \end{aligned} \quad (16)$$

$$\begin{aligned}
A_i^{n=0}(L, E, r_x) &= 2\{2\mu[E - V_i(\infty)]\}^{1/2}(z_i^2 - b^2)^{1/2} \\
&= 2(2\mu E)^{1/2}(r_x^2 - b^2)^{1/2} \\
&\quad - \frac{(2\mu/E)^{1/2} r_x^2 V(r_x)}{E(r_x^2 - b^2)^{1/2}} \\
&\quad + o\left(\frac{1}{E^{3/2}}\right). \quad (17)
\end{aligned}$$

Up to terms of second order, these expressions cancel identically when the subtractions are made to form the functions Θ_d and A_d .

The terms of lowest order in $1/E$ can now be expressed concisely if we use an average and a difference potential in the form

$$V_a = \frac{1}{2}[V_1(r) + V_2(r)], \quad (18)$$

$$V_d = \frac{1}{2}[V_1(r) - V_2(r)] = \Delta V/2.$$

The angles and actions can be written in the reduced form

$$\begin{aligned}
\tau_a(b; E^{-1}) &= E\Theta_a(b, E) = -b \int_b^\infty \frac{dV_a}{dr} \frac{dr}{(r^2 - b^2)^{1/2}} \\
&\quad + o\left(\frac{1}{E}\right), \quad (19)
\end{aligned}$$

$$\begin{aligned}
\alpha_a(b; E^{-1}) &= \left(\frac{E}{2\mu}\right)^{1/2} A_a(b, E) = \int_b^\infty \frac{dV_a}{dr} \frac{r^2 dr}{(r^2 - b^2)^{1/2}} \\
&\quad + o\left(\frac{1}{E}\right), \quad (20)
\end{aligned}$$

$$\begin{aligned}
\tau_d(b; E^{-1}) &= E\Theta_d(b, E) = -b \int_b^{r_x} \frac{dV_d}{dr} \frac{dr}{(r^2 - b^2)^{1/2}} \\
&\quad + o\left(\frac{1}{E}\right), \quad (21)
\end{aligned}$$

$$\begin{aligned}
\alpha_d(b; E^{-1}) &= \left(\frac{E}{2\mu}\right)^{1/2} A_d(b, E) = \int_b^{r_x} \frac{dV_d}{dr} \frac{r^2 dr}{(r^2 - b^2)^{1/2}} \\
&\quad + o\left(\frac{1}{E}\right). \quad (22)
\end{aligned}$$

To this approximation - ignoring terms in $1/E$ - it suffices to use the single impact parameter b in these expressions.

To evaluate τ_a and α_a it is necessary to know the average potential $V_a(r)$ over its whole range from b to ∞ , but the difference potential in τ_d and α_d need only be known inside r_x . Using a quadratic expression for the difference potential

$$\begin{aligned}
V_d(r) &= (r - r_x)V_d'(r_x) + (r - r_x)^2 V_d''(r_x)/2 \\
&= r_x V_d'(r_x) \left[\left(\frac{r}{r_x} - 1\right) + \frac{C}{2} \left(\frac{r}{r_x} - 1\right)^2 \right], \quad (23)
\end{aligned}$$

where

$$C = r_x V_d''(r_x)/V_d'(r_x),$$

and taking

$$b/r_x = \beta = 1 - \gamma,$$

we may evaluate τ_d and α_d and expand them about $b_x = r_x$:

$$\begin{aligned}
\frac{\tau_d(b)}{r_x V_d'(r_x)} &= -C\beta(1 - \beta^2)^{1/2} - (1 - C)\beta \\
&\quad \times \ln\left(\frac{1 + (1 - \beta^2)^{1/2}}{\beta}\right) \\
&= -(2\gamma)^{1/2} \left(1 - \frac{7\gamma}{12} \dots\right) + \frac{1}{3} C (2\gamma)^{3/2} \dots \quad (24)
\end{aligned}$$

and

$$\begin{aligned}
\frac{\alpha_d(b)}{r_x^2 V_d'(r_x)} &= \frac{1}{3} C (1 - \beta^2)^{1/2} (1 + 2\beta^2) + \frac{1}{2} (1 - C) \\
&\quad \times \left[(1 - \beta^2)^{1/2} + \beta^2 \ln\left(\frac{1 + (1 - \beta^2)^{1/2}}{\beta}\right) \right] \\
&= (2\gamma)^{1/2} \left(1 - \frac{11\gamma}{12} \dots\right) - \frac{1}{3} C (2\gamma)^{3/2} \dots \quad (25)
\end{aligned}$$

By differentiating Eq. (24), one can see that $\tau_d(b)$ has a vertical slope at $b = r_x$. These expansions are valid for b near r_x and have the property that successive derivatives of $V(r)$ first appear in terms with higher and higher powers of γ . Unfortunately, they cannot be relied upon except close to r_x because the successive coefficients such as C [Eq. (23)] may be of the order of magnitude of unity; convergence then requires that γ be quite small. One very important aspect of this vertical slope at $b = r_x$ is that, even with repulsive potentials, the classical trajectories $\Theta_{II} = \Theta_1 - 2\Theta_d$ and $\Theta_{IV} = \Theta_a - \Theta_d$ will possess minima. Upon forming the elastic differential cross section, then, a rainbowlike structure will usually appear (this depends of course on the magnitude of the coupling matrix), and a smaller effect of the same sort may sometimes be expected in the inelastic scattering pattern. This phenomenon is discussed later in the text.

Both the inelastic and the elastic differential scattering cross sections may show an interference pattern due to the two trajectories. In the semiclassical approximation, the reduced inelastic cross section $\rho_{ij} = \theta \sin\theta \sigma_{ij}(\theta)$ can be written

$$\rho_{12} = \omega^{-1} |g_{1II}(\theta, E) + g_{1V}(\theta, E)|^2, \quad (26)$$

with its elastic counterpart

$$\rho_{11} = \omega^{-1} |g_{1I}(\theta, E) + g_{1II}(\theta, E)|^2. \quad (27)$$

The factor ω^{-1} is a symmetry factor; for ground-

state $\text{He}^+ + \text{He}$, where the crossing is in the states of g (gerade) symmetry only, and only He^+ (or only He^*) is detected, $\omega = 4$. For the $\text{He}^+ + \text{Ne}$ case, ω is equal to unity.

The reduced scattering amplitudes can be written

$$g_J(\theta, E) = [P_J(E, b_J)\rho_J(\theta, E)]^{1/2} \times \exp\{i[\hbar^{-1}A_J(\theta, E) - \gamma_J]\}, \quad (28)$$

where the magnitude $P_J\rho_J$ is the product of a transition probability P_J with an ordinary classical reduced cross section from the trajectory of Eqs. (6):

$$\rho_J(\theta, E) \cong \frac{1}{2} \frac{db_J^2(\tau)}{d \ln \tau}. \quad (29)$$

The functions $b_J(\tau)$ are the impact parameters responsible for scattering at the reduced angle τ through each of the trajectories T_J ; they may differ considerably from each other. They are found by simple inversion of the function $\tau_J(b)$.

The probabilities of transition P_J may be approximated by the Landau-Zener formula, at least in the limit where $(r_x - b)/\delta r_x$ is large. They are

$$\begin{aligned} P_I(E, b_I) &= e^{-2w_I}, \\ P_{II}(E, b_{II}) &= (1 - e^{-w_{II}})^2, \\ P_J(E, b_J) &= e^{-w_J}(1 - e^{-w_J}) \quad (J = III, IV), \end{aligned} \quad (30)$$

with

$$\begin{aligned} w_J(E, b_J) &= \frac{2\pi V_{12}(r_x)^2}{\hbar \Delta V (2E/\mu)^{1/2}} \left(1 - \frac{V_x}{E} - \frac{b_J^2}{r_x^2}\right)^{-1/2} \\ &\cong \frac{2\pi \delta r_x (\mu/2)^{1/2} V_{12}(r_x)}{\hbar E^{1/2} [1 - b_J^2/r_x^2]^{1/2}}. \end{aligned} \quad (31)$$

Near the threshold the Landau-Zener formula fails, and a more refined treatment is called for. Equations (30) have been connected with the S matrix in another paper.⁹

The inelastic scattering cross sections are then written as

$$\begin{aligned} \rho_{12} &= \omega^{-1} \{P_{III}(E, b_{III})\rho_{III}(\theta, E) + P_{IV}(E, b_{IV})\rho_{IV}(\theta, E) \\ &\quad + 2P_{III}^{1/2}(E, b_{III})\rho_{III}^{1/2}(\theta, E)P_{IV}^{1/2}(E, b_{IV})\rho_{IV}^{1/2}(\theta, E) \\ &\quad \times \cos[2\pi N(\theta, E)]\}, \end{aligned} \quad (32)$$

where the interference oscillations appear as a term proportional to $\cos 2\pi N(\theta, E)$ with the index number N determined by the difference in the action integrals, that is,

$$2\pi N_{12}(\theta, E) = \hbar^{-1}[A_{III}(\theta, E) - A_{IV}(\theta, E)] - \gamma + \pi. \quad (33)$$

A similar expression to Eq. (32) may be written for the elastic scattering with the interference terms proportional to

$$2\pi N_{11}(\theta, E) = \hbar^{-1}[A_I(\theta, E) - A_{II}(\theta, E)] - \gamma. \quad (34)$$

According to Thorson and Boorstein,¹⁰ the phase

constant is $\gamma = \pi/2$.

The difference in the action integrals, Eqs. (33) and (34), may be identified with the difference in impact parameters for scattering at angle θ through the use of a general theorem⁸ connecting the angular momentum L , the action integral A , and the deflection function Θ . In the case of interest here, the deflection function Θ is equal to the angle of scattering θ , but in other cases such as rainbow scattering it may have the opposite sign. Since we have

$$\frac{(2\mu E)^{1/2}}{\hbar} b_J(\theta, E) = L_J(\theta, E) = \frac{\partial A_J(\theta, E)}{\partial \theta}, \quad (35)$$

it follows that

$$\Delta b(\theta, E) = \frac{2\pi \hbar}{(2\mu E)^{1/2}} \frac{\partial N}{\partial \theta}, \quad (36)$$

where N is the indexing number of the oscillations. Therefore, the oscillations seen on both the elastic and inelastic scattering cross sections yield information about the difference in the impact parameters for the two trajectories observed at the angle θ .

We will now go on to present the semiquantal formulas for the two-state elastic and inelastic scattering and in a later section present the results for calculating the cross sections by the various methods.

B. Quantal Treatments: Exact and Approximate

The semiclassical procedure presented above is obviously approximate, and it is important to test its validity and examine alternative approximations. For this purpose, we consider the quantal equations for a two-state system

$$\frac{d^2 G_{11}}{dr^2} + \left(k_1^2 - \frac{l(l+1)}{r^2} - U_{11}\right) G_{11} = U_{12} G_{21}, \quad (37a)$$

$$\frac{d^2 G_{21}}{dr^2} + \left(k_2^2 - \frac{l(l+1)}{r^2} - U_{22}\right) G_{21} = U_{12} G_{11}, \quad (37b)$$

where

$$U_{ij} = \frac{2\mu}{\hbar^2} V_{ij}(r),$$

and where the boundary conditions must provide properly for conservation of flux. The desired output is the 2×2 S matrix as a function of E and l ; because of its unitarity (conservation of particles) and symmetry (microscopic reversibility), there are really only three independent real parameters,⁹ a magnitude A ($|A| \leq 1$) and phases η_1 and η_2 :

$$\begin{aligned} S_{11} &= (1 - A^2)^{1/2} e^{2i\eta_1}, \quad S_{22} = (1 - A^2)^{1/2} e^{2i\eta_2}, \\ S_{12} &= S_{21} = iA e^{i(\eta_1 + \eta_2)}. \end{aligned} \quad (37c)$$

Since A itself may oscillate, it is sometimes con-

venient to factor it in the form

$$A = q(l, E) \sin \delta(l, E), \quad (37d)$$

where q and δ are slowly varying functions (the factorization is not unique, and one of these functions is arbitrary).

The S -matrix elements can be computed at each l orbital angular momentum quantum number ($\hbar l = L$) for a given set of initial and final energies and potentials, and the scattering amplitudes or cross sections are then obtained by the partial wave summation. At the energies involved here (~ 100 eV), the number of l values required for solution with a given set of conditions extends into the hundreds; hence approximations are demanded by computer cost. It is, however, desirable that exact solutions to Eqs. (37) be available so that comparisons may be made with the approximate solutions.

If the transition probabilities are small, the distorted wave (DW) approximation¹¹ may be utilized. One first obtains G_{1i}^0 and G_{2i}^0 as solutions to Eqs. (37) with $U_{12} = 0$; the associated phase shifts are η_{1i}^0 . We have assumed wave functions with the asymptotic form

$$G_{ii}^0(r) \sim \left(\frac{\pi k_i r}{2} \right)^{1/2} [\cos \eta_{1i}^0 J_{l+1/2}(k_i r) + (-1)^l \times \sin \eta_{1i}^0 J_{l-1/2}(k_i r)]. \quad (38)$$

Then the off-diagonal element S_{12} is of the form (37c) with the zero-order phase shifts η_{1i}^0 and a first-order estimate for A

$$A^{(1)} = \frac{2}{(k_1 k_2)^{1/2}} \int_0^\infty G_{1i}^0(r) U_{12}(r) G_{2i}^0(r) dr. \quad (39)$$

From the S -matrix elements, the cross sections may then be computed by

$$\sigma_{ij}(\theta) = |f(\theta)|^2 = |(2ik_1)^{-1} \sum_l (2l+1)(S_{ij}^l - \delta_{ij}) \times P_l(\cos \theta)|^2. \quad (40)$$

One distinct disadvantage of the DW approximation is that it does not preserve the unitary property of the S matrix. One method to remove this feature is to renormalize the S matrix¹² so that $\sum_j |S_{ij}^l|^2 = 1$. For the cases involved here, this renormalization did not institute any significant changes. It does, however, allow the DW method to be extended to larger transition probabilities $|S_{ij}^l|^2$. Nevertheless, when the factor q of Eq. (37d) approaches or exceeds unity, the DW approximation should be abandoned.

Another often-used approximation¹³ for calculating the transition probabilities is the Stueckelberg-Landau-Zener (SLZ) method.¹⁴ Here, transitions are assumed to depend only on the interaction pa-

rameters evaluated at the crossing point r_x where the initial- and final-state energies are equal. The inelastic transition probabilities are given by

$$|S_{12}^l|^2 = 4p_l(1-p_l) \sin^2(\delta_l + \gamma), \quad (41)$$

where $p_l = e^{-w}$ is the usual Landau-Zener formula in which w is given by Eq. (31), and δ_l by the quadratures

$$\delta_l = \int^{r_x} g_+^{1/2} dr - \int^{r_x} g_-^{1/2} dr, \quad (42)$$

where

$$g_\pm = \frac{1}{2}(f_1 + f_2) \pm \frac{1}{2}[(f_1 - f_2)^2 + (4U_{12})^2]^{1/2},$$

with

$$f_{1,2} = k_{1,2}^2 - U_{11,22} - \frac{(l + \frac{1}{2})^2}{r^2}. \quad (43)$$

The phase constant γ has been mentioned previously in Eq. (33). Since δ_l customarily extends through several multiples of π , oscillatory structure is contained within $\sin^2 \delta_l$, and hence the transition probabilities $|S_{12}^l|^2$. The SLZ inelastic cross sections are computed via Eqs. (37c) and (40) with

$$A^l = p_l^{1/2}(1-p_l)^{1/2} \sin(\delta_l + \gamma). \quad (44)$$

For both the DW and SLZ methods, the elastic differential cross sections may be calculated by Eq. (40) with the S -matrix elements of Eq. (37c).

In principle, the SLZ treatment is less reliable than the DW method, because the former approximates the potentials and U_{12} by certain constant values evaluated at the crossing point, whereas the latter method allows correctly for their functional behavior at large distances from r_x . Both of these approximations are formulated in such a way as to be correct at moderate-to-high energies, but the DW method should continue to be valid much higher in the energy scale because of this more realistic formulation. It appears that there is quite a large range of energies where both of these approximations are reliable, and in this region the SLZ method is simpler to apply. Under these conditions, the semiclassical method almost always leads to results identical with those of the SLZ method. The semiclassical approach is conceptually helpful in viewing the cross sections as arising from a combination of trajectories with interference effects caused by their mixing at some common angle θ .

At energies extremely close to threshold, where k_2 approaches 0, the DW approximation breaks down because Eq. (39) exceeds unity, violating unitarity of the S matrix. In this region the SLZ result, in contrast, remains formally satisfactory in that its value for A approaches 0 instead of ∞ , but it is in fact somewhat incorrect because it does not allow for tunneling. Near threshold, therefore, an improved approximation or a numerical solution is called for. This region has been studied by Bykovskii

TABLE I. He⁺-Ne potential and crossing parameters. All values are in atomic units.

a_1	21.1
a_2	0.678
a_3	12.1
a_4	0.170
a_5	0.667
r_x	2.02
E_x	0.530
$V_{12}(r_x)$	0.00819
$V_1'(r_x)$	-1.044
$V_2'(r_x)$	-0.134

and his associates¹⁵ and recently by Delos and Thorson.^{7,16}

CALCULATIONS

Before we can perform calculations via the several methods described above, we must first choose potential forms that are physically realistic so that qualitative comparisons can be made with experimental data. In this case, we will utilize potential functionalities that approximately reproduce the He⁺+Ne elastic and inelastic data.¹ They are given by

$$\begin{aligned} V_1(r) &= a_1 r^{-1} e^{-r/a_2}, \\ V_2(r) &= (a_1 r^{-1} - a_3) e^{-r/a_2} + 16.8 \text{ eV}, \\ V_{12}(r) &= a_4 e^{-r/a_5}, \end{aligned} \quad (45)$$

and are intended to reproduce the elastic and He⁺+Ne → He⁺+Ne(2p⁵3s) inelastic reaction.¹⁷ In Table I, we give the various values for a_1, a_2, \dots, a_5 and also the pertinent crossing parameters. Figure 1 illustrates $V_1(r)$ and $V_2(r)$. The adiabatic calculations of Michels¹⁸ are also shown. Here we see that the adiabatic potential follows $V_1(r)$ for $r > r_x$ and

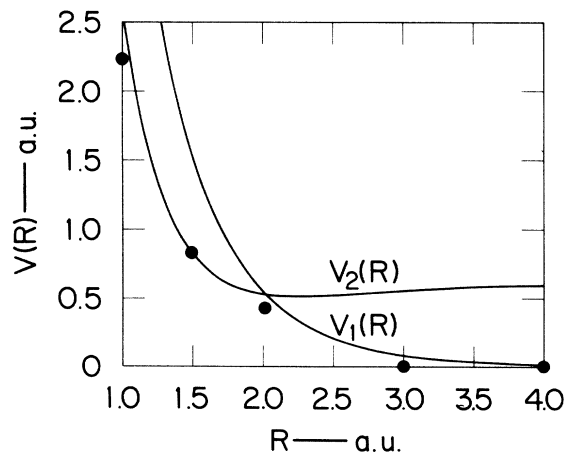


FIG. 1. The diabatic potentials for He⁺-Ne from which the calculations were made. The solid circles are from the theoretical calculations of Michels (Ref. 18) on the first excited state (adiabatic).

then switches to $V_2(r)$ for $r < r_x$. This is as expected for a crossing between potential curves of the same symmetry. Of particular significance is that the functionality of $V_1(r)$, Eq. (45) and its parameters, also reproduces the elastic data.

In the computations, the coupled radial wave equations, Eqs. (37), were solved by using the same starting conditions and Numerov integration scheme as did Lane and Geltman¹⁹ with the S matrix being formed by the methods of Lester and Bernstein.¹⁹ Checks were made at several energies and l values with the amplitude density program of Secrest and Johnson.²⁰ The real and imaginary parts of the S matrix were found to agree to four significant figures. The DW solution, Eqs. (38) and (39), to the S matrix was formed by using a one-channel Numerov integration procedure. Gaussian quadratures were utilized in the SLZ method, and the phase constant of Eq. (41) was set equal to zero. More will be said about this phase constant later, since it appears to be a function of δ_l . All phase shifts η_l were calculated by the JWKB method.

Using the potentials given by Eq. (45) and the parameters of Table I, we will now calculate the deflection functions of Eqs. (1)–(6) for the elastic and inelastic trajectories. These deflection functions will then be related to the elastic and inelastic cross sections.

The two elastic deflection functions at 70.9 eV are shown in Fig. 2. The deflection function $\Theta_I = \Theta_1$ corresponds to trajectory T_I where the particles follow potential $V_1(R)$ everywhere. Trajectory T_{II} yields the deflection function $\Theta_{II} = \Theta_1 - 2\Theta_d$ and corresponds to the particles following potential $V_1(r)$

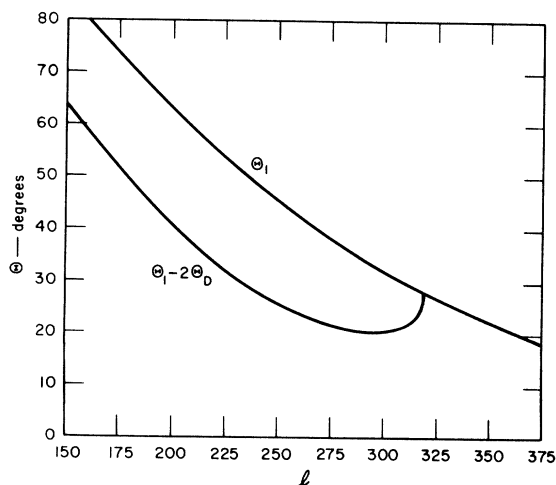


FIG. 2. Deflection functions for the two potentials of Fig. 1 versus the orbital angular momentum quantum number l ($l \approx bk$). The kinetic energy of the ground state is $E_1 = 2.606$ a.u. (70.9 eV) and of the excited state $E_2 = 1.988$ a.u. (54.1 eV).

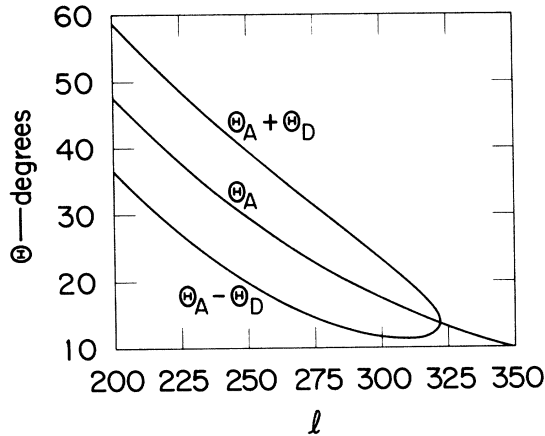


FIG. 3. Average deflection function and the average plus and minus the difference deflection function for the same conditions as in Fig. 2.

to r_x , switching to $V_2(r)$ for $r < r_x$, and then transferring back to $V_1(r)$ at r_x on the outward passage.

Several characteristics should be noted. The first is the perpendicular slope of Θ_{II} at $l_x = 322$. This was predicted by the expansions in Eq. (24). Secondly, it should be pointed out that Θ_{II} possesses a minimum at $\Theta = 21^\circ$; $\tau = E\theta = 1490$ eV deg. If the coupling matrix is of a magnitude such that it allows transfer to potential $V_2(r)$ at r_x , then the possibility arises for the existence of rainbow structure so that there will be a sharp peak on the elastic cross sections. More importantly, this phenomenon does *not* require that $V_1(r)$ or $V_2(r)$ have a minimum within $r < r_x$. Also we should note that at a given angle θ greater than θ_x , $\theta_x = \theta(l_x)$, the observed scattering will result from the particles following two trajec-

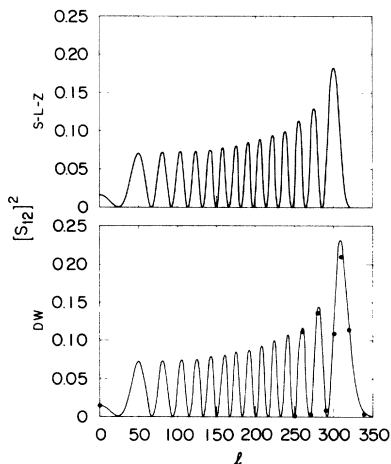


FIG. 4. Comparison between the SLZ and DW transition probabilities at 70.9 eV. The solid circles on the DW results are from two-state close-coupled calculations.

tories which have two different impact parameters or l values. Therefore, at the common angle θ , an interference effect will result, and oscillations will be observed on the elastic cross sections for angles $\theta > \theta_x$. The spacing of the oscillations may be related to the difference in impact parameters by Eq. (36).

Figure 3 shows the deflection functions corresponding to the inelastic case. Here trajectory T_{III} with the deflection function $\Theta_{III} = \Theta_A + \Theta_D$ corresponds to the particles following potential $V_1(r)$ until the outward passage where at r_x they switch to potential $V_2(r)$. In trajectory T_{IV} with the deflection function $\Theta_{IV} = \Theta_A - \Theta_D$, the particles switch from potential $V_1(r)$ to $V_2(r)$ at r_x on the inward passage and then remain on $V_2(r)$. As in Fig. 2, we see that there is a sharp break at l_x , and then for $l < l_x$ there is the possibility of the particles following two different paths so that for scattering to angles $\theta > \theta_x$ there will be interference effects, and oscillatory structure will appear on the inelastic cross sections. As in the elastic case, Eq. (36) relates the difference in impact parameters to the spacings of the oscillatory structure. Also, there is a possibility of the rainbow-type structure caused by the minimum in Θ_{IV} . However, this requires tunneling through a potential barrier; hence, the weighting probability would be small. It should be noted that, because of the nature of the transition probabilities, the inelastic scattering will have a sharp threshold angle that corresponds to θ at l_x . Also, in almost all cases, one will find that $\theta_x^{el} \neq \theta_x^{inel}$.

To compute the elastic or inelastic cross sections, Eq. (40), the transition probabilities must first be calculated. Here, we have used the potential parameters of Table I and, at an energy of 70.9 eV, we have calculated the transition probabilities via the SLZ, DW, and close-coupled two-state methods. They are presented in Fig. 4.

On the upper portion of the graph, the SLZ results, Eqs. (41) and (43), are displayed; the phase constant γ was set equal to zero. The SLZ transition probabilities have the expected oscillatory structure and begin quite abruptly at $l_x = 322$, since there is no allowance for tunneling. For comparison, the DW results are shown on the lower part of Fig. 4. Immediately it is apparent that there is a shift in phase of the oscillatory structure when the two methods are compared with one another. At

TABLE II. Inelastic totals. All values are in atomic units.

Energy	SLZ	DW
0.919	0.645	0.874
2.606	0.567	0.729
7.350	0.365	...

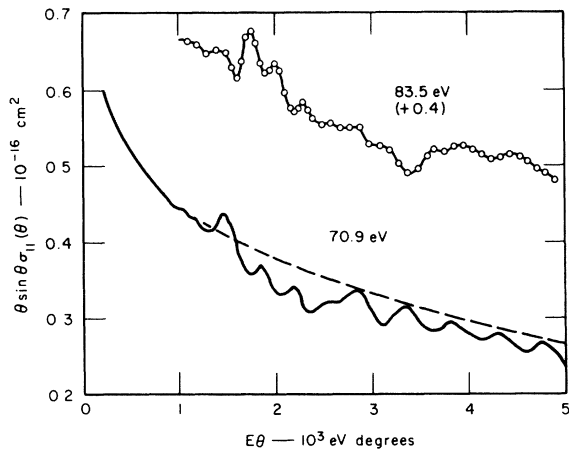


FIG. 5. 70.9-eV elastic differential cross sections computed using the distorted wave transition probabilities. The dashed line is a one-state calculation assuming no inelastic transitions. For a comparison, the 83.5-eV experimental data (Ref. 1) are shown and have been shifted by a factor of +0.4.

and around l_x , the SLZ shift amounts to a $\pi/4$ phase factor which is consistent with the predictions of Thorsen and Boorstein.¹⁰ It should also be noted that the $\pi/4$ phase factor slowly approaches zero as the impact parameter is decreased. The transition probabilities then are almost in perfect agreement. We have also checked the DW calculations by per-

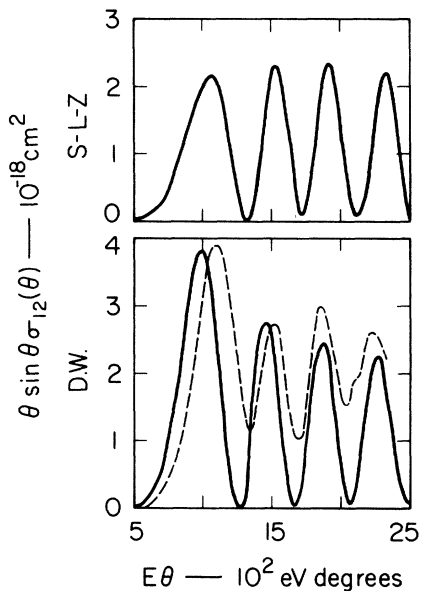


FIG. 6. Corresponding inelastic cross sections to Fig. 4. The experimental data (Fig. 7) for the same energy have been superimposed with dashed lines upon the DW results.

forming some coupled two-state calculations (the solid circles of Fig. 4). When plotted on the DW results, it is found that the calculations are quite good around the threshold region, and that the only differences are at the maxima. This is as expected, since the DW method will tend to overestimate the transition probabilities because it does not allow for back coupling. The peak positions seem well reproduced.

We may also calculate the total inelastic cross sections from the two sets of transition probabilities by the use of

$$Q_{12} = \frac{\pi}{k_1^2} \sum_l (2l+1) |S_{12}|^2 \quad (46)$$

and then compare the results. They are given in Table II along with some other energies at which calculations were made. We see that the DW transition probabilities yield cross sections that are slightly larger than the SLZ ones. In this case, this is because the SLZ method does not allow for tunneling and cuts off an important contribution to the total cross section.

We may now go on to calculation of the elastic cross sections. They are shown in Fig. 5 along with some experimental data¹ at 83.5 eV. The solid line corresponds to using DW transition probabilities with JWKB phase shifts in Eq. (40). For comparison, the dashed line is for the pure elastic case. As predicted by the deflection functions in Fig. 2, we observe a sharp peak at $\tau = 1450$ eV deg and oscillatory structure for $\theta > \theta_x$. The spacing of the oscillations, which is related by Eq. (36) to the difference in impact parameters or l values, is also consistent with Fig. 2. For a comparison, the cross sections of the nearest experimental energy to 70.9 eV are displayed. We see a similar type of structure with a sharp peak followed by oscillatory structure. It appears the qualitative features are well reproduced by a simple two-state calculation.

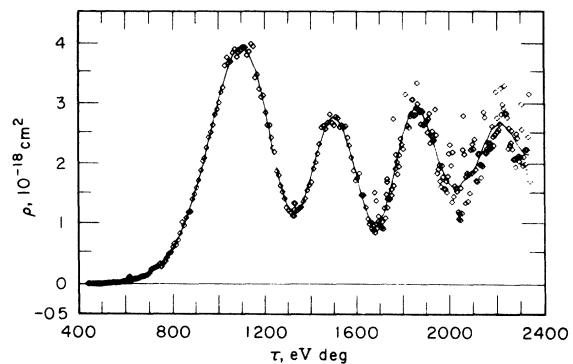


FIG. 7. Experimental inelastic cross sections at 70.9 eV of Coffey, Lorents, and Smith (Ref. 1) for the $\text{He}^+ + \text{Ne}$ system.

We have also calculated the elastic cross sections by the semiclassical method described in Eqs. (30)–(34). The cross sections are well reproduced in both their magnitude and frequency of oscillations for $1000 \text{ eV deg} < \tau < 2500 \text{ eV deg}$. As expected, about θ_x the semiclassical method breaks down. What must be remembered is that the semiclassical method provides a practical physical insight into the collision process.

Figure 6 presents the SLZ and DW inelastic cross sections. The dashed line is a reproduction of the 70.9 eV experimental data¹ shown in Fig. 7. As predicted by the classical deflection functions of Fig. 3, we see a rapid rise when the threshold is reached, followed by oscillatory structure. These oscillations again are directly related to the difference in impact parameters for the particles following either trajectory T_{III} or T_{IV} and scattered to the common angle θ . The main difference between the DW and SLZ calculations is found in the first maximum where the SLZ calculation differs slightly in its threshold characteristics and in its magnitude. The following SLZ peaks also display a slight shift which is due to the phase factor question in the transition probability. At larger and larger angles, the two methods become identical. The calculations were also performed by the semiclassical method of Eqs. (30)–(33), and at $\tau \gtrsim 1250 \text{ eV deg}$ they agreed almost perfectly with the SLZ method. For impact parameters close to r_x , as in the elastic case, we get spurious results from the lack of smoothness in the special deflection functions, Fig. 3. The qualitative features of the experimental data shown by the dashed line in Fig. 6, and displayed more completely in Fig. 7, are well reproduced by the two-state calculation. The magnitude of the minima differs but this is believed to be because more channels are opening up for $b < b_x$; hence there is dampening of the experimental oscillations. It is encouraging to see that the general features are reproduced by the two-state calculation. Also, it is heartening to know that the SLZ method and the semiclassical method work so well in predicting not only the amplitude but also the positions of oscillatory structure and their threshold values. It indeed allows for a rapid estimation of the crossing parameters from the experimental data.

CONCLUDING REMARKS

In the calculation of the transition probabilities via the SLZ and DW methods, the phase constant γ of Eq. (41) was found to vary between 0 and $\pi/4$ as l approached l_x . The $\pi/4$ factor for l values close to l_x is in accordance with the predictions of Thorson and Boorstein.¹⁰ From calculations at other

energies, however, we did notice that γ was a function of l and, upon closer investigation, found it correlated with δ_l . This functionality has been roughly parametrized for this system as

$$\gamma_l \cong (\pi/4) e^{-\delta_l/20},$$

where γ_l and δ_l are in radians. Other calculations²¹ of γ for the general case will soon be available.

We must also note that the semiclassical formulas relating the oscillatory scattering patterns to the difference in impact parameters, Eq. (36), can be verified. From a plot of the index number N ($N=0, 1, 2, \dots$ for the maxima as θ increases) versus τ for the inelastic calculations of Fig. 6, the slope yields a $\Delta b(\theta)$ of 0.36 a. u. or a $\Delta l(\theta)$ of 64. In Fig. 3, the average $\Delta l(\theta)$ for $l < l_x$ in the angular range of interest is about 63.

The main drawback to the semiclassical formulas is that they are not valid for impact parameters close to r_x and hence do not yield cross sections that are valid in the threshold regions. Possibly, much of this disadvantage can be removed by smoothing the special deflection functions in the regions about b_x and by using a suitable extension of the SLZ formulas through to the tunneling region.

We also observe that on the elastic cross sections there was a sharp peak which was predicted by the semiclassical method. This structure is akin to rainbow scattering but is not dependent upon any intermolecular potential possessing a minimum; the only requirement is that there is an inelastic channel available for reaction.

Part of the amazingly good agreement between the semiclassical and DW treatments may rest in the fact that the crossing point is well localized for this case. An estimate of the effective width of the crossing may be calculated from

$$\delta r_x = V_{12}(r_x)/\Delta V'(r_x).$$

For the crossing described, we find δr_x to be equal to 0.01, which indicates a very-well-defined crossing point.

In conclusion, we believe it is reasonable to say that the semiclassical method makes it possible to understand and analyze the experimental measurements of the elastic and inelastic differential cross sections. If the crossing point is well defined, the method should yield quantitative estimates of the potential parameters which can then be used in more rigorous calculations.

ACKNOWLEDGMENT

The authors wish to thank Dr. B. R. Johnson for providing his two-state computer program so that computer checks could be made.

*The authors wish to thank the National Aeronautics and Space Administration and an Atholl McBean Fellowship

(REO) for providing the necessary funds.

¹F. T. Smith, R. P. Marchi, W. Aberth, D. C.

Lorents, and O. Heinz, Phys. Rev. 161, 31 (1967); D. Coffey, Jr., D. C. Lorents, and F. T. Smith, *ibid.* 187, 201 (1969); F. T. Smith, H. H. Fleischmann, and R. A. Young, Phys. Rev. A 2, 379 (1970); and W. Aberth, O. Bernardini, D. Coffey, Jr., D. C. Lorents, and R. E. Olson, Phys. Rev. Letters 24, 345 (1970).

²R. P. Feynman, Rev. Mod. Phys. 20, 367 (1948); and P. Pechukas, Phys. Rev. 181, 166 (1969).

³K. W. Ford and J. A. Wheeler, Ann. Phys. (N. Y.) 7, 259 (1959); and N. G. Van Kampen, Physica 35, 70 (1967).

⁴D. R. Bates and A. R. Holt, Proc. Roy. Soc. (London) A292, 168 (1966); L. Willets and S. J. Wallace, Phys. Rev. 169, 84 (1968); R. McCarroll and A. Salin, J. Phys. B 1, 163 (1968); and J. C. Y. Chen and K. M. Watson, Phys. Rev. 174, 152 (1968).

⁵B. A. Lippmann and J. Schwinger, Phys. Rev. 79, 469 (1950).

⁶M. H. Mittleman, Phys. Rev. 122, 499 (1961); S. A. Lebedoff, *ibid.* 165, 1399 (1968); and M. L. Goldberger and K. M. Watson, *Collision Theory* (Wiley, New York, 1964).

⁷J. B. Delos and W. R. Thorson (unpublished).

⁸C. Lehmann and G. Leibfried, Z. Physik 172, 465 (1962); F. T. Smith, R. P. Marchi, and K. G. Dedrick, Phys. Rev. 150, 79 (1966); F. T. Smith, J. Chem. Phys. 42, 2419 (1965).

⁹F. T. Smith, in *Lectures in Theoretical Physics: Atomic Collision Processes*, edited by S. Geltman, K. T. Mahanthappa, and W. E. Brittin (Gordon and Breach, New York, 1969), Vol. XIC, p. 95.

¹⁰W. R. Thorson and S. A. Boorstein, in *Fourth International Conference on the Physics of Electric and Atomic Collisions, Abstracts of Papers* (Science Bookcrafters, Hastings-on-Hudson, 1965), p. 218.

¹¹See, for example, N. F. Mott and H. S. W. Massey, *The Theory of Atomic Collisions* (Clarendon, Oxford, England, 1965), Chap. XIII.

¹²R. B. Bernstein, A. Dalgarno, H. S. W. Massey, and I. C. Percival, Proc. Roy. Soc. (London) A274, 427 (1963); R. E. Olson and R. B. Bernstein, J. Chem. Phys. 50, 246 (1969).

¹³Some of the latest papers are T. A. Green and R. E. Johnson, Phys. Rev. 152, 9 (1966); M. Matsuzawa, J. Phys. Soc. Japan 25, 1153 (1968); R. P. Marchi, Phys. Rev. 183, 185 (1969); L. P. Kotova, Zh. Eksperim. i Teor. Fiz. 55, 1375 (1968) [Soviet Phys. JETP 28, 719 (1969)].

¹⁴E. C. G. Stueckelberg, Helv. Phys. Acta 5, 369 (1932); L. Landau, Soviet Phys. 2, 46 (1932); C. Zener, Proc. Roy. Soc. (London) A137, 696 (1933).

¹⁵V. K. Bykhovskii, E. E. Nikitin, and M. Ya. Ovchinnikova, Zh. Eksperim. i Teor. Fiz. 47, 750 (1964) [Soviet Phys. JETP 20, 500 (1965)].

¹⁶J. B. Delos, Ph.D. thesis, MIT, 1970 (unpublished).

¹⁷It should be noted that we have recently found that the crossing point and interaction matrix derived from the experimental data are in good agreement with the results of V. Sidis, who, from *ab initio* calculations, obtained $r_x = 1.86$ a.u. and $H_{12} = 0.096$ a.u. V. Sidis, Ph.D. thesis, University of Paris, 1970 (unpublished).

¹⁸H. H. Michels, NBS Technical Note 438, edited by M. Krauss (U. S. GPO, Washington, D. C., 1967), p. 115.

¹⁹W. A. Lester, Jr. and R. B. Bernstein, J. Chem. Phys. 48, 4896 (1968); N. F. Lane and S. Geltman, Phys. Rev. 160, 53 (1967).

²⁰D. Secrest and B. R. Johnson, J. Chem. Phys. 45, 4556 (1966).

²¹J. B. Delos (private communication).

Production and Detection of the Orientation of Ions by Spin-Exchange Collisions with Optically Pumped Rubidium

H. M. Gibbs and G. G. Churchill

Bell Laboratories, Murray Hill, New Jersey 07974

(Received 24 November 1970)

Radio-frequency spectroscopy of ions has been performed on the $(\text{Sr}^{87})^+$, $(\text{Cd}^{111})^+$, and $(\text{Cd}^{113})^+$ ground states utilizing spin-exchange collisions with optically pumped rubidium atoms for both producing and detecting the orientation.

I. INTRODUCTION

The ion ground-state orientations reported here are the first to be both produced and detected via spin-exchange collisions with polarized atoms. This technique requires no ion resonance radiation, which is often difficult to produce. Conceivably, the technique could be applied to negative ions, most of which have no resonance radiation. Also, only small quantities of material are required, making feasible an extension to rare isotopes. The

technique is rather general, since no resonant collisions are required for detection. However, the precision of the technique is not competitive with the ion-storage collision technique,¹ because of the short relaxation times in the unconfined high-density discharge; this may also restrict the method to S states. The possible extension of the technique to a measurement of g values and hyperfine structures of any S-state ion is suggested by the observation of Zeeman resonances in Sr^+ (which is representative of the group-II A ions) and Cd^+